

REFINEMENT OF THE 3D-SCANNING TOOLCHAIN FOR THE CHARACTERIZATION OF AEROSPACE STRUCTURES - REPORT

L. van Bruegge, S. J. Koeberle, M. Hornung
Institute of Aircraft Design, Technical University of Munich,
Boltzmannstraße 15, 85748 Garching, Germany

Abstract

We present a 3D-scanning toolchain for the characterization of UAVs. It is capable of extracting airfoils, the fuselage and geometric characteristics, like the dihedral and chord length. This report summarizes the abilities of the toolchain and assesses the accuracy of both the scanning and extraction process. Three different 3D-scans of the UAV *15tol* are compared to the reference design. Sections of all scans are extracted and compared geometrically and aerodynamically to the design airfoil. Additionally, the aircraft is reconstructed in CATIA V5 and XFLR5 to compare overall flight behavior and geometric deviation.

Keywords

Remotely Piloted Aircraft System; RPAS; Unmanned Aerial System; UAS; Unmanned Aerial Vehicle; UAV; 3D-Scanning; Geometry Extraction

1. INTRODUCTION

Previously, Çetin [1] and van Brügge [2] presented a 3D-scanning toolchain for the characterization of Unmanned Aerial Vehicles (UAVs). In cooperation with Moritz Thiele¹ and Fabian Sturm², a conference paper for the DLRK 2021 was submitted on this topic [3]. In contrast to [1] and [2], the paper covered a wider range of aerospace structures which can be characterized using the developed toolchain, such as morphing wings and propeller geometries. During research, it became clear that there are still open questions and missing functionalities regarding the toolchain.

First of all, an assessment of its accuracy was never made. Hence, it is still unclear where the deviation from the design geometry originates. Possible reasons range from the scanning resolution to the scanning process itself. The implementation could also be based on partially wrong assumptions. Furthermore, the implementation can be improved: Features like the smoothing and fitting process developed in [2] still have some issues handling the leading edge. In this report, we present results generated by the improved toolchain. These results indicate which tolerances and deviations should be expected.

2. SHORT INTRODUCTION OF THE 3D-SCANNING TOOLCHAIN

The toolchain can be separated into two main parts: the scanning and the extraction process. The 3D-scanning is done manually using any 3D-scanner. For a standard aircraft extraction, the aircraft is scanned in several segments, which are then digitally assembled afterwards. The scanning resolution should be as accurate as possible. Optionally, the flaps can be actuated and extracted as well. In this case, the flaps

have to be actuated in direction of the hinge line for the algorithm to work properly.

In order to extract all sections automatically after scanning, the aircraft has to be exported as a text file consisting of 3D data points. The point cloud of the aircraft is then aligned and sectioned. Additionally, all sections are fitted: The fuselage section can be fitted to either a circle, an ellipse or a superellipse; the wing can be fitted to a spline interpolation or a CST parameterization using Bernstein polynomials. For a more detailed description, refer to [1, 2].

3. ASSESSMENT OF THE POINT CLOUDS OF DIFFERENT 3D-SCANNERS

For the assessment process of the 3D-scans, a cooperation between the Institute of Aircraft Design³ and the Institute of Geodesy⁴ was founded, to improve the qualities of the 3D-scans and the scanning process. Three different 3D-scanners were tested and compared - the *HandySCAN 700* by *CREAFORM* in combination with the *MAXshot 3D* also by *CREAFORM*, the *RTC360* by *Leica* and the *AT901-MR* Laser-tracker by *Leica*. The *CloudCompare* [4] software was chosen for the comparison of the point clouds.

As a first case study, the UAV *IMPULLS* was scanned using the *HandySCAN 700* and compared to its CAD model. Afterwards, the UAV *15tol* was scanned using the three 3D-scanners listed above. Again, the scans are compared to the design model and additionally the scans of the *HandySCAN 700* and the *RTC360* to the scan of the Laser-tracker.

3.1. Accuracy of the 3D-Scanners

The volumetric accuracy of the different coordinate measurement systems and 3D-scanners are stated in Tab. 1 and 2.

¹Technical University of Munich, Institute of Aircraft Design

²Technical University of Munich, Institute of Aircraft Design

³Technical University of Munich

⁴Technical University of Munich

As can be seen, the accuracy of the *HandySCAN 700* can be greatly increased by using the scanner in combination with the coordinate measurement system *MAXshot 3D*. However, the Lasertracker has a significantly higher resolution than the *HandySCAN 700*. The *RTC360* has a lower resolution, too.

HandySCAN 700 (A)	MAXshot 3D (B)	Combination A & B
0.020 mm + 0.060 mm/m	0.025 mm/m	0.020 mm + 0.025 mm/m

TAB. 1. Accuracy of the 3D-scanners of CREAFORM

Lasertracker AT901-MR	RTC360
$\pm 10 \mu\text{m}$	1.0 mm + 10 ppm

TAB. 2. Accuracy of the 3D-scanners of Leica

This difference in accuracy is explained by the different methods used for the point cloud creation. The *RTC360* and the *HandySCAN 700* are both laser scanners. Laser scanning is a direct scanning method where the direct reflection of a laser beam from the object is measured to obtain surface information. Most deviations can be explained by inaccurate positioning of reference points or the scanner itself. In contrast, the *AT901-MR* uses a *lasertracking* method, where the exact positioning of a handheld probe is tracked by a second transmitter. This second system emits laser beams which are then reflected by the probe to measure its position. The actual scanning of the object differs depending on the probe and its application. In this case, the probe is a handheld laser scanner which then uses the same method as mentioned above for the point cloud generation. Issues determining the exact position of the probe may occur if the probe is occluded by the object.

3.2. Measurement of the UAV *IMPULLS*

The main UAV of interest is the *15tol* by the Institute of Aircraft Design. In contrast to the UAV *IMPULLS*, standard aircraft manufacturing tolerances of less than 1 mm were not achieved. Therefore, a comparison of the point cloud scanned from the *IMPULLS* aircraft to its reference design is made to be able to assess the deviations of *15tol* in more detail. The aircraft fuselage and tail were scanned using the *CREAFORM HandySCAN 700*. For the wings, a combination of the *CREAFORM HandySCAN 700* and *CREAFORM MAXshot 3D* was used. The design geometry is a surface loft of the CAD model in CATIA V5 [5]. The comparison of the point cloud to the loft is presented in Fig. 1. The point cloud is filtered such that only points with a maximum distance of ± 5 mm between the scanned data and the CAD loft are presented, in order to exclude outliers and to compute a more precise point distribution in the main area of interest. This filtered data set includes 90% of the complete point cloud.

As shown in Fig. 1, the fuselage and the v-tail have several areas where the scanned points are more than 5 mm away from the loft. The tail and the fuselage were scanned only

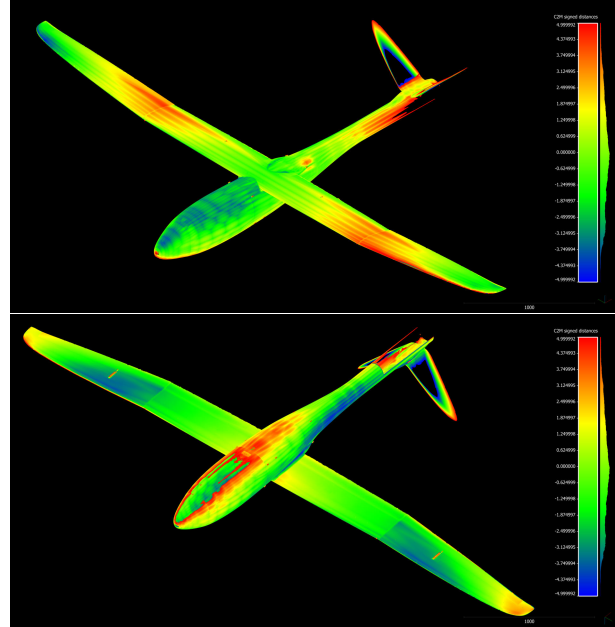


FIG. 1. Comparison of the point cloud of the aircraft IM-PULLS to its CAD model

using the *HandySCAN 700*, and not the combination of both *CREAFORM* scanners. Both large deviations are explained by an imperfect scan assistance model. In the case of the fuselage, the deviations are explained by the size of the fuselage and the positioning on a desk (see Fig. 2 in [3]). Due to the desk, the required scanning distance to the bottom surface could sometimes not be met, while also ensuring that enough tracking markers were visible. The v-tail was scanned separately from the rest of the aircraft, such that the size of its scan poses no problem. Nonetheless, there are large deviations compared to the CAD model. These stem from the problem of generating an assistance model for the top and the bottom sides of the v-tail, since the tracking markers visible at switching positions like the leading edge are relatively sparse.

Most deviations are in a range of ± 1.5 mm, especially in the wing area, which demonstrates the scanning improvement when the assistance model is generated using the *MAXshot 3D*, instead of just the *HandySCAN 700*. Even at the wing tip, the deviations are less than 3 mm. Distances between the scanned points and their respective counterparts in the reference CAD model are shown in Fig 2.

3.3. Measurement of the UAV *15tol*

Three different 3D-scans are available, thanks to the Institute of Geodesy. These are compared to the CAD model and to each other, in order to estimate the manufacturing tolerances and the accuracy of the scanning process.

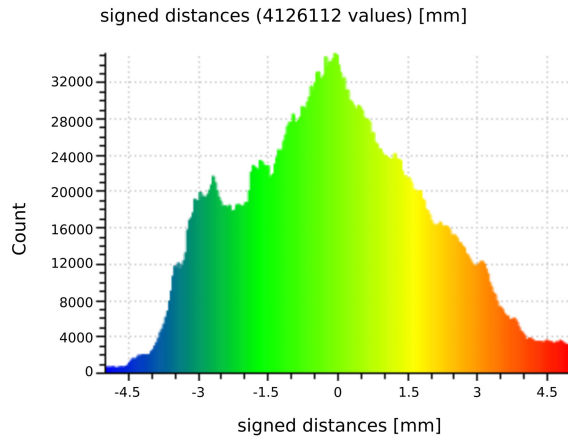


FIG. 2. Distances between the scanned points and their respective counterparts in the reference CAD model of the UAV IMPULLS

3.3.1. Comparison of the Point Clouds to the CAD Model

Comparison to the complete CAD Model

The point clouds generated by the Lasertracker and the HandySCAN 700 were compared to the CATIA V5 model. The first point cloud was chosen for its accuracy and the second one is the only available 3D-scan which contains a complete fuselage. Figure 3 shows the comparison of the point clouds to the CATIA V5 model of the 15tol. To get a better alignment of the point clouds, the aircraft was split along its symmetry plane. Again, both clouds were filtered to only contain points within a range of 5 mm absolute distance to the CAD model. The filtered clouds consist of 95.9% of the original data set for the Lasertracker and 98.2% for the HandySCAN 700.

In case of the Lasertracker, the fuselage of the 3D-scan is the part which shows the greatest deviations. It is assumed that this area was only roughly scanned in comparison to the wing and tail. Both scans show a relatively low mean point distance of 0.65 mm to 0.7 mm. This can also be seen in the two histograms in Fig. 4. Interesting to see is that the histogram for the HandySCAN 700 scan contains two peaks, one at 0 mm and one at 2.5 mm. In contrast, the histogram of the Lasertracker scan has a more even distribution and most of the deviations stay between -1.5 mm and 2.5 mm.

Comparison of the Wing Section

To rule out an inaccurate alignment, the wing was segmented and compared to the CAD model (see Fig. 5). As before, a histogram of the point distance distribution is shown in Fig. 6. Again, the point clouds were filtered to be within an absolute distance of ± 5 mm to the CAD model. This results in point clouds of 99.0% of the original data set for the Lasertracker, 99.5% for the HandySCAN 700 and 98.4% for the RTC360. The HandySCAN 700 and the Lasertracker show less deviation in this comparison. Thus, it is assumed that a large part of the deviations of the comparison above resulted from the misalignment of both point clouds. However, for the HandySCAN 700, the two peaks are still visible and even more distinct than in the comparison of the whole aircraft.

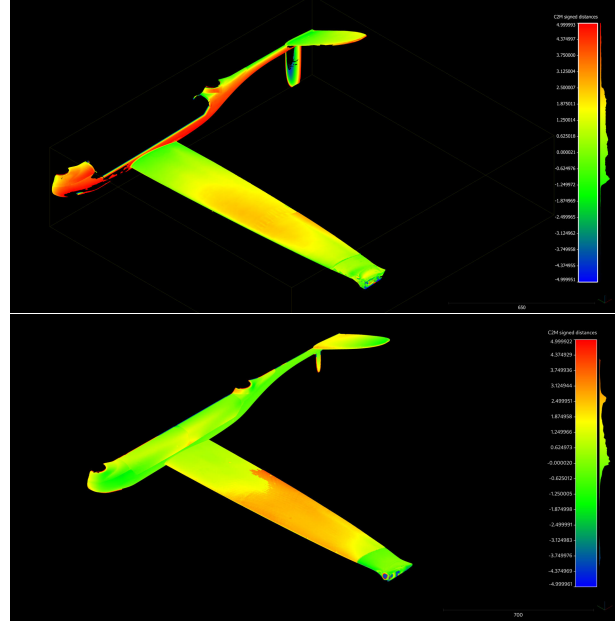


FIG. 3. Deviation of the 3D-scan from the Lasertracker (top) and the HandySCAN 700 (bottom) from the CAD model of the 15tol

Mean distances and standard deviations of all scans were also computed. Overall, all used 3D-scanners tend to overestimate the object, resulting in a volume larger than the reference volume, and a positive mean distance. The computed mean distances and standard deviations in millimeters are shown in Tab. 3.

Scanner Type	Mean Distance	Std. Deviation
Lasertracker	0.4733 mm	1.5259 mm
HandySCAN 700	1.1768 mm	1.317 mm
RTC360	0.822 mm	1.7984 mm

TAB. 3. Mean distances and standard deviations for the comparisons of the scanned wing to its CAD model

As expected, the Lasertracker has the lowest mean distance, however its standard deviation is significantly higher than the one of the HandySCAN 700. This also explains why the filtered point clouds of the HandySCAN 700 scans retain the highest percentage of points from the original data set.

3.3.2. Comparison of the Point Clouds to Each Other

For an additional comparison, the 3D-scan of the Lasertracker is compared to the other 3D-scans. These comparisons are presented in Fig. 7 and 8. As before, the clouds were filtered. However, this time, the distances between the two point clouds are always positive, so filtering was done one-sided only. For the RTC360 the previous 5 mm filter cutoff distance was used. For the HandySCAN 700, this value had to be raised to 10 mm in order to retain enough points. This results in point clouds of 94.4% of the original data set for the

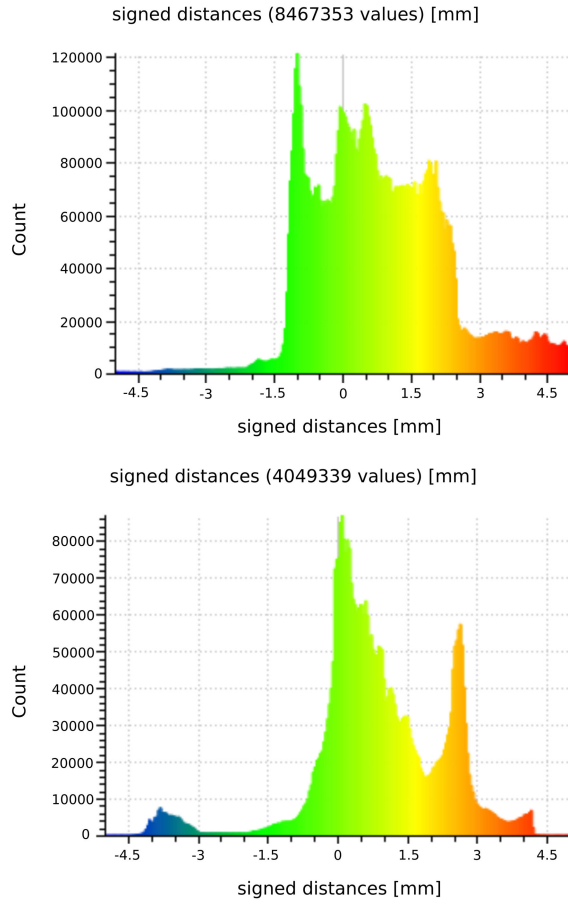


FIG. 4. Distribution of the point distances of the scan of the Lasertracker (top) and the HandySCAN 700 (bottom) compared to the CAD reference model of 15tol

HandySCAN 700, and of 90.9% for the *RTC360*. The smallest volume of the point cloud is generated by the Lasertracker, since both 3D-scan comparisons result in distances greater than 0 mm. Interestingly, the Lasertracker underestimated some points of the original CAD model (see Fig. 3 and 4). In order to result in negative distances to the CAD model and only positive distances in the comparison with each other, all 3D-scanners apparently underestimate the CAD loft in the same areas. This indicates manufacturing inaccuracies in these areas. Additionally, the *HandySCAN 700* clearly has a larger deviation than the *RTC360*. The highest deviations are on the bottom side near the wing tip and the tail. Generally, the wing of the point cloud generated using the *HandySCAN 700* displays a different deflection than the other two scans. The root and tip of the wing show higher deviations than the middle of the wing. It is unclear where this deflection error comes from. A possible explanation is that the UAV was assembled for the first time ever for the scan using the *HandySCAN 700*, and directly disassembled afterwards. In contrast, the other two scans were done over a time span of several months where the UAV stayed assembled the whole time and settling and creeping processes could occur.

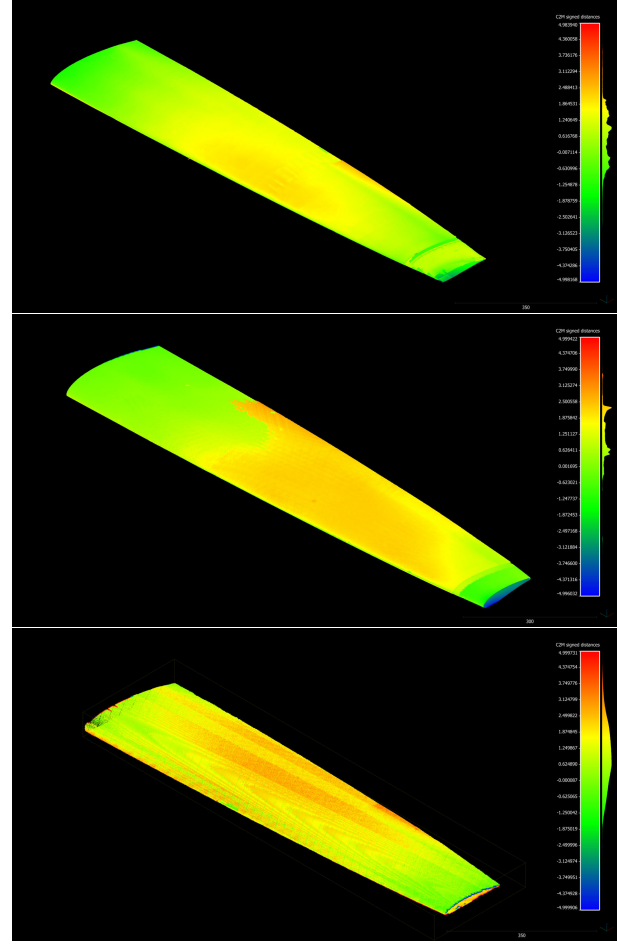


FIG. 5. Comparison of the wing segment to the CATIA V5 model for the 3D-scan of the Lasertracker (top), the HandySCAN 700 (middle) and the RTC360 (bottom)

4. ASSESSMENT OF THE GENERATED WING AND TAIL SECTIONS

4.1. Capabilities of the Fitting Process

The scans have no smooth surface due to reflection artifacts or misaligned positioning. In order to smooth these defects, a shape function multiplied with a Bernstein polynomial (see Eq. 1) is fitted to the whole section. This is done by first splitting the section into an upper and lower half. The shape function generates a standard airfoil shape, which is then configured with the Bernstein polynomial to adjust e.g. the thickness of the foil and the camber. Fitting each of the halves to Eq. 1 with the order $n=8$ is done using a linear least-squares approximation.

For this fitting to succeed, the scan has to fulfill several conditions (see below). Otherwise, the extracted section can not be smoothed. Several error sources are presented. In every fig-

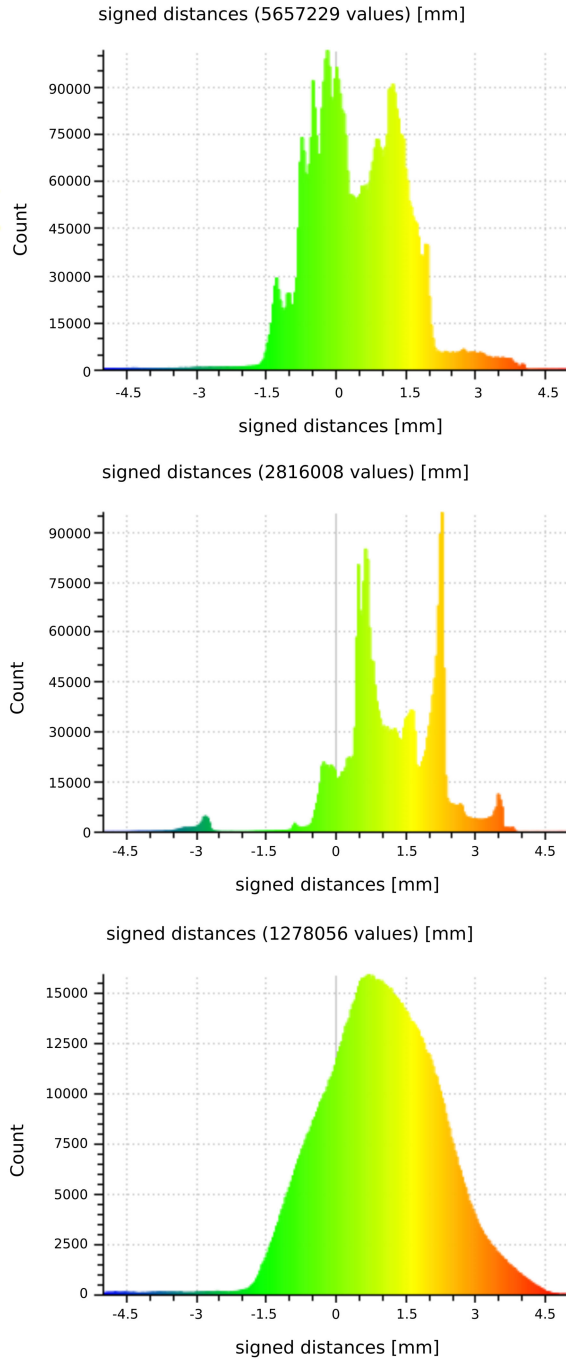


FIG. 6. Distribution of the point distances of the 3D-scan of the Lasertracker (top), the HandySCAN 700 (middle) and the RTC360 (bottom), compared to the reference CAD design

ure, the extracted section points are depicted using red dots while the fitted airfoil is a blue line.

$$(1) F(x) = \sqrt{x} \cdot (1-x) \cdot \sum_{i=0}^n f\left(\frac{i}{n}\right) \cdot \binom{n}{i} \cdot x^i \cdot (1-x)^{n-i}$$

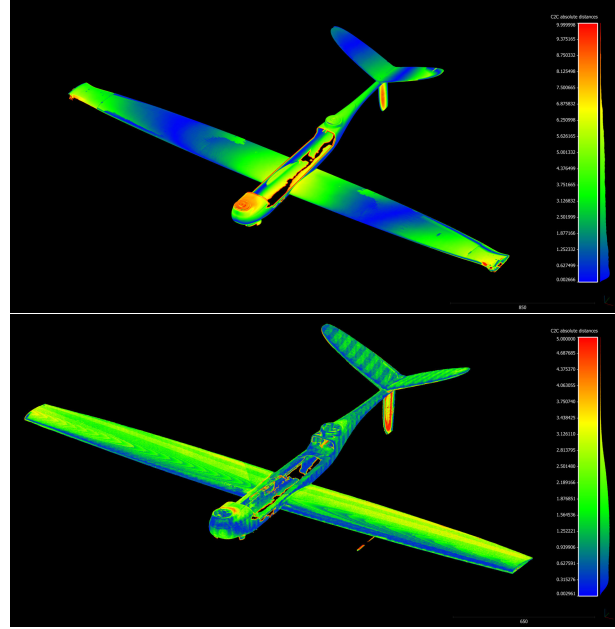


FIG. 7. Comparison of the 3D-scans of the HandySCAN 700 (top) and the RTC360 (bottom) to the 3D-scan of the Lasertracker

4.1.1. Least-Square Oscillation

This type of error is difficult to fix since it is inherent to every least-square fitting problem using polynomials. Depending on the distribution of the points, the computed polynomial oscillates around the extracted points. This problem occurs mostly at wing tips where the resolution and accuracy of the scan is lower. An oscillating result of the fitting process is presented in Fig. 9. It is assumed that these oscillations occur due to a high order of the polynomial. This problem could be fixed by choosing a polynomial of a lower degree, or another fitting method. However, if a lower polynomial degree is used, the top surface may not be represented accurately in all cases.

4.1.2. Several Surfaces Detected

If the scanner has detected several surfaces in the scanning process, the fitting will fail. This is usually caused by movement of the scanned object during the scanning process, or internal structures of the wing like servo holders. In this case, the least-square fit tries to average the surfaces in this region and chooses the center line. This effect can be observed in Fig. 10 at the leading edge.

A rather extreme example is shown in Fig. 11, where an unsuitable 3D-scanner was chosen for the sectioning. This scanner rebuilds the surfaces out of several parallel slices, which are then averaged during the fitting process.

4.1.3. Invalid Orientation of the Section

The orientation is an important factor for the fitting process. After the alignment of the point cloud, the main axes are known, but not the exact orientation of the aircraft. Before the

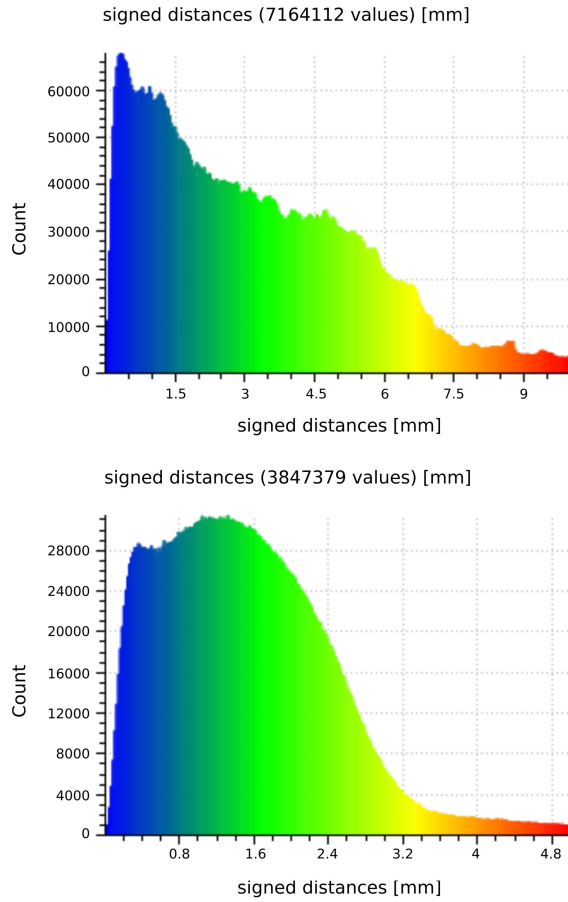


FIG. 8. Point cloud distances of the HandySCAN 700 (left) and the RTC360 (right) compared to the Lasertracker

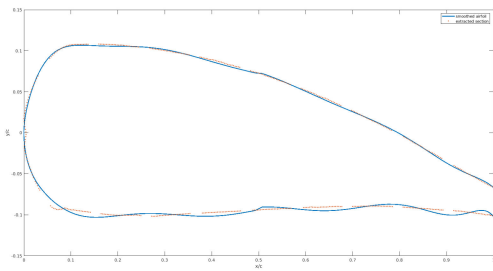


FIG. 9. Oscillating least-square fitting

fitting, the algorithm determines whether the airfoil is upside down, and whether the leading and trailing edge are swapped. In these cases the airfoil is mirrored along the corresponding axis. If an invalid leading edge position was not properly detected, the fitting will fail as shown in Fig. 12.

This failure has two reasons. First of all, the section is never rotated after the fitting process. Secondly, the underlying shape function is depending on the correct rotation. The shape function is presented in Eq. 2. At point (0,0), it gen-

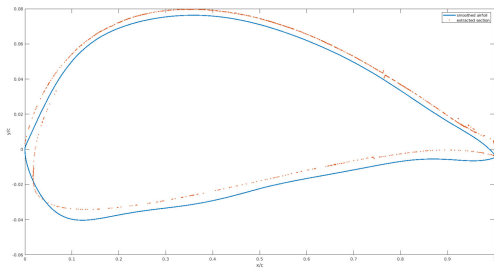


FIG. 10. Errors due to several detected surfaces

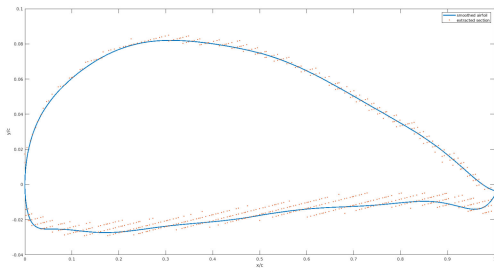


FIG. 11. Errors due to unsuitable averaging of sections

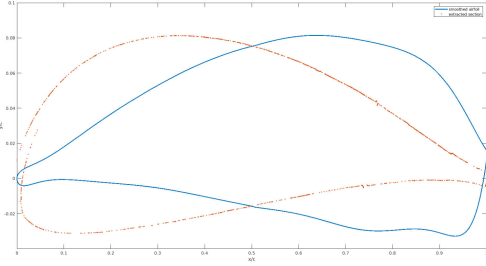


FIG. 12. Failed fitting due to a wrong orientation beforehand

erates a vertical tangent (corresponding to the leading edge) while the point (1,0) has a pointed edge (corresponding to the trailing edge). Since the foil is misaligned in this error condition, the actual leading edge becomes pointy while the original pointy part of the trailing edge becomes round.

$$(2) \quad s = \sqrt{x} \cdot (1 - x)$$

4.1.4. Points at the Trailing Edge

The fitting is able to deal with airfoils containing a trailing edge thickness. In this case, the airfoil is not completely pointy, but has a small vertical edge instead. This phenomenon can be usually traced back to manufacturing inaccuracies. Since the shape function as described in Eq. 2 always ends in (1,0), the halves containing a thickness at the trailing edge are translated such that the last point of the half lies on (1,0). Therefore, points of the vertical edge must be removed beforehand. This is done automatically in the algorithm as well. However, it

is possible that not all points of the trailing edge are detected. In that case, the translation is smaller than needed and the edge fitting is invalid (see Fig. 13).

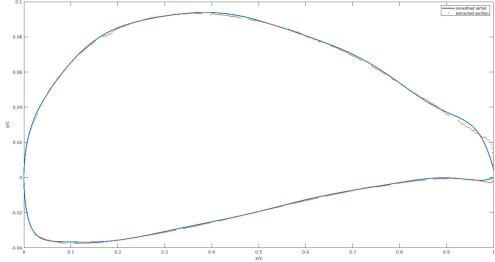


FIG. 13. Failure due to remaining points at the trailing edge

4.1.5. Sectioning only one Side of the Wing

The fitting algorithm expects a complete airfoil. If this is not the case, the fitting will fail and both fitted lines will not approximate the section. The reason for this behavior is that the fitting algorithm tries to separate the section anyway, leading to both separated parts not containing a complete representation of the section. An example is shown in Fig. 14.

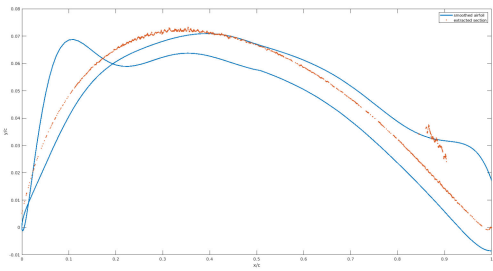


FIG. 14. Fitting of partial data

4.1.6. Successful Fitting

If all requirements are met, the fitting produces a result similar to Fig. 15.

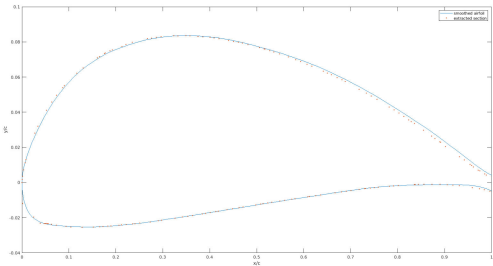


FIG. 15. Successful Bernstein polynomial fitting

4.2. Geometric Deviations compared to the Design Profile

The sections generated from the 3D-scans of the Lasertracker and the *HandySCAN 700* were compared to the design profile of the *15tol*. This design profile is a SD7032 airfoil which was then thickened to 1 mm at the trailing edge. Overall, the generated airfoils are always thicker than the design profile. This can be explained by manufacturing tolerances and the accuracy of the scanning process.

4.2.1. Assessment of the Wing Sections

Several sections spanning from the wing root to the tip were extracted. Unfortunately, not all sections met the requirements of the fitting process (see Sec. 4.1) and could not be compared. Here, some resulting examples are presented. As mentioned above, standard tolerances could not be met and the accuracy of the aircraft is unknown. Thus, it is impossible to attribute the deviations to any specific cause, but it is assumed that most deviations can be classified as manufacturing tolerances since both scanners generate similar results.

Sections of the HandySCAN 700 For the *HandySCAN 700*, three sections were compared to the design profile, one at the wing root, one at the wing tip, and one near the airspeed probe. The plots of all sections and their differences to the design airfoil are presented in Fig. 16 to 18.

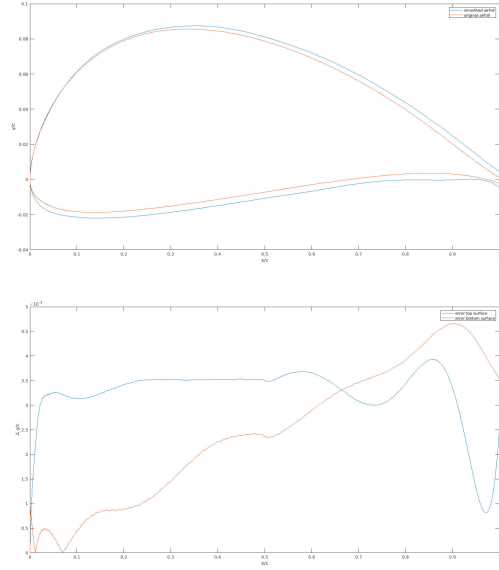


FIG. 16. Top: Comparison of the section at 110 mm, generated by the *HandySCAN 700*, to the design airfoil. Bottom: The normalised difference between both airfoils.

As shown, the absolute difference between both airfoils increases towards the wing tip. Additionally, the error at the bottom side of the airfoil is greater than the error on the top

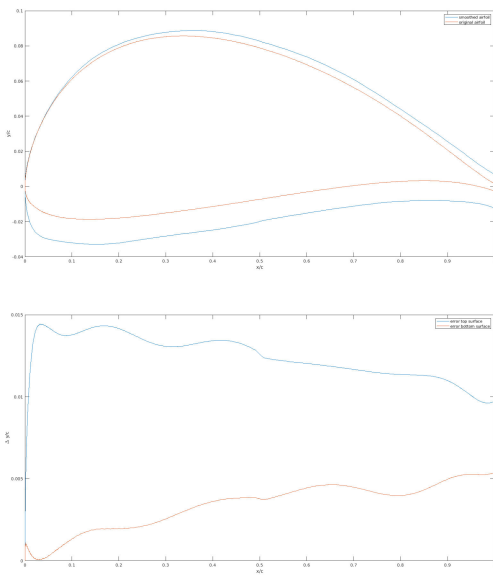


FIG. 17. Top: Comparison of the section at 1010 mm, generated by the HandySCAN 700, to the design airfoil. Bottom: The normalised difference between both airfoils.

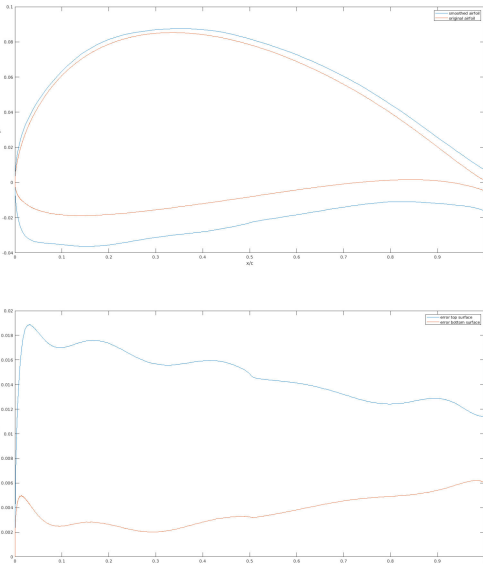


FIG. 18. Top: Comparison of the section at 1350 mm, generated by the HandySCAN 700, to the design airfoil. Bottom: The normalised difference between both airfoils.

side. Oscillations as presented in Sec. 4.1.1 occur primarily in the front part of the bottom side, while oscillations on the top side are rare. The designed trailing edge thickness of 1 mm could not be met for any of the sections.

The mean error stays within $2.218 \cdot 10^{-3}$ normalised to the

chord length for the wing root and $8.695 \cdot 10^{-3}$ for the wing tip. Maximum differences are between $4.658 \cdot 10^{-3}$ and $1.9094 \cdot 10^{-2}$.

Section of the Lasertracker Scan Only one section of the 3D-scan generated using the Lasertracker could be compared to the design profile, because the scan has a faulty leading edge where two surfaces are detected (see Fig. 10). This section and its normalised difference to the design profile are plotted in Fig. 19.

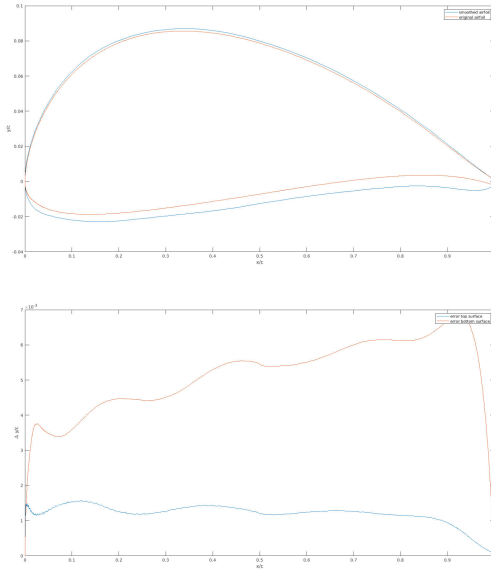


FIG. 19. Top: Comparison of the section at 110 mm, generated by the Lasertracker, to the design airfoil. Bottom: The normalised difference between both airfoils.

In this section, the mean error is $2.715 \cdot 10^{-3}$ and the maximal error $6.844 \cdot 10^{-3}$. This deviation is greater than the one of the HandySCAN 700 section, which can be explained by the faulty fitting at the trailing edge, where not all points of the edge could be deleted (see Sec. 4.1.4). If this part of the foil is removed, the mean error is reduced to $2.344 \cdot 10^{-3}$, which is similar to the mean distance of the comparison using the section generated by the HandySCAN 700.

4.2.2. Assessment of the V-Tail Sections

The v-tail was sectioned as well, and compared to its design profile. In this case, the design profile is a HT14 airfoil which was thickened about 10% near the wing root, to fit the servo for the flap. One section for each scanner was chosen and compared. The results are plotted in Fig. 20 and 21.

The section generated using the HandySCAN 700 is significantly thicker than the design airfoil. However, it is assumed that this inaccuracy stems from the scanning process, since the airfoil of the Lasertracker has a similar thickness as the design profile. The mean distances for both airfoils are the

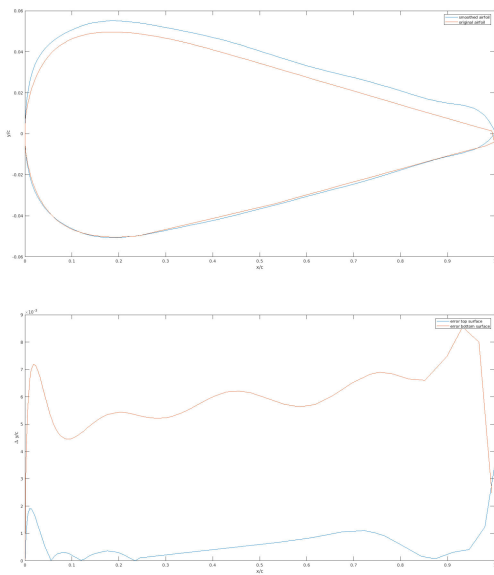


FIG. 20. Top: Comparison of the v-tail section at 50 mm, generated by the HandySCAN 700, to the design airfoil. Bottom: The normalised difference between both airfoils.

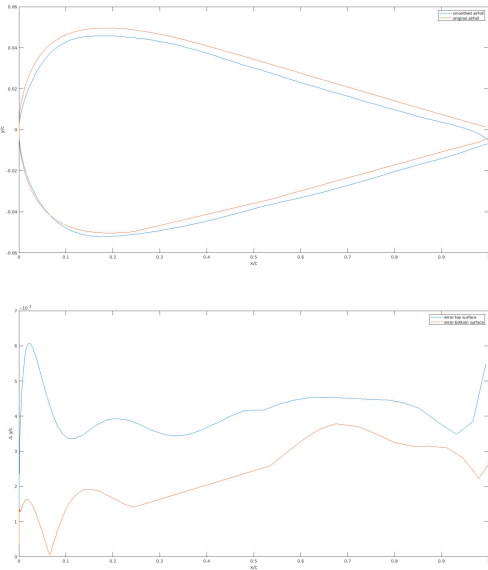


FIG. 21. Top: Comparison of the v-tail section at 50 mm, generated by the Lasertracker, to the design airfoil. Bottom: The normalised difference between both airfoils.

same nevertheless, since the airfoil of the Lasertracker was translated too much during the fitting process. This can occur if the leftmost point of the airfoil is not the leading edge, since this point defines the center of the coordinate system. Over the complete v-tail, the mean error stays between $2.87 \cdot 10^{-3}$

and $6.9 \cdot 10^{-3}$. The maximum difference is not comparable because the design airfoil contains a vertical edge at the trailing edge which distorts this value.

4.2.3. Assessment of the Vertical Tail Sections

Like the v-tail, the vertical tail sections yield a high deviation. However, this time the extracted airfoil is always significantly smaller than the design profile. Since the scanners tend to overestimate the object, most of this deviation is attributed to manufacturing tolerances. An exemplary section of the *HandySCAN 700* is shown in Fig. 22.

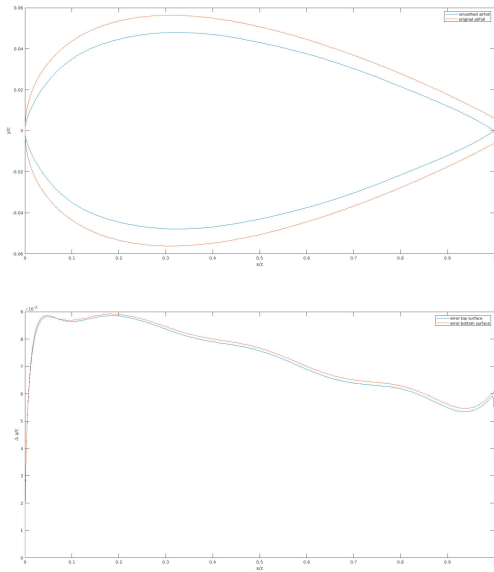


FIG. 22. Top: Comparison of a section of the vertical tail, generated by the HandySCAN 700, to the design airfoil. Bottom: The normalised difference between both airfoils.

The mean difference of the vertical tail stays between $7.115 \cdot 10^{-3}$ and $1.1 \cdot 10^{-2}$, and its maximum difference ranges up to $1.63 \cdot 10^{-2}$. However, this high value does also result from a faulty fitting at the leading edge. No vertical tail section could be extracted from the Lasertracker scan, due to a different orientation in space.

4.3. Aerodynamic Assessment of the extracted Sections

In the following, the aerodynamic behavior is compared to the design profile. One section of the *HandySCAN 700* scan and the Lasertracker scan each was chosen, and compared using the low-fidelity aerodynamic software XFLR5 [6]. Three different exemplary Reynolds numbers were chosen for the comparison: $6 \cdot 10^4$, $16 \cdot 10^4$ and $5 \cdot 10^5$. These cover almost the complete flight regime of the wing. $5 \cdot 10^5$ is the Reynolds number which is reached at the wing root during a flight with 20 m/s, while $6 \cdot 10^4$ is reached at the wing tip during slow flight. The polars corresponding to these Reynolds numbers are shown in the following figures. In these, the polars

of the design airfoil are presented in red, the polars of the *HandySCAN 700* scan in green and the polars of the Lasertracker scan in blue.

4.3.1. Aerodynamic Behavior of the Wing

Overall, the aerodynamic behavior resembles the one of the design airfoil. Thus, the geometric difference has no major influence on it. Plots of both the lift- to drag-coefficient, as well as the lift-coefficient to angle of attack (α) are presented in Fig. 23. As can be seen, the polars of the section gen-

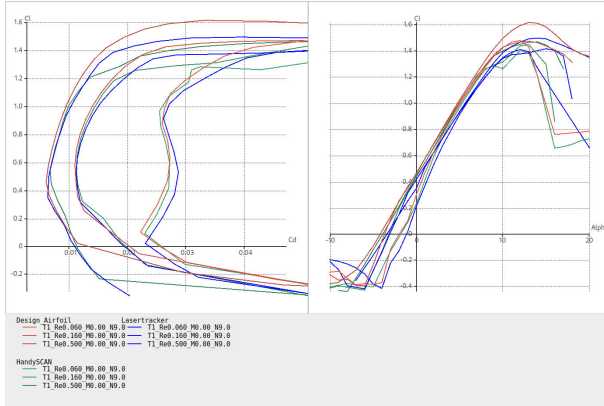


FIG. 23. Comparison of the polars of the wing to the design profile at three different Reynolds numbers

erated by the *HandySCAN 700* approximate the design airfoil pretty well to a lift-coefficient of 1.2. Beyond that, the lift-coefficient is significantly smaller than the one of the design airfoil. In contrast, the polars of the section generated using the Lasertracker reach higher c_l -values. However, $c_{l,max}$ was not reached either, and in areas of low lift-coefficients the section of the *HandySCAN 700* data approximates the design polar even better. In addition, the $c_{l,\alpha}$ -coefficient was approximated rather well by both sections, and even though $c_{l,max}$ was not reached, the airfoils show similar α_{max} -values. For the plot of the pitching moment coefficient (c_m) to α , the section of the *HandySCAN 700* data shows a similar tendency as the design airfoil, while the coefficient of the Lasertracker data section is too high at positive angles of attack. This is possibly explained by the imperfect fitting of the trailing edge, which is shown in Fig. 19. The plot for the pitching moment coefficient is presented in Fig. 24.

4.3.2. Aerodynamic Behavior of the V-Tail

The aerodynamic behavior of the v-tail was compared in the same way as the wing. The v-tail has a different flight regime compared to the wing, so an additional polar was added with a Reynolds number of $35 \cdot 10^3$. The polars of the lift coefficients are presented in Fig. 25.

In the low Reynolds area, both sections approximate the airfoil well. Unfortunately, the bucket of the design airfoil at a Reynolds number of $6 \cdot 10^4$ could not be generated using any of the extracted sections. In the high Reynolds area, both airfoils do not generate the $c_{l,max}$ -value of the design airfoil,

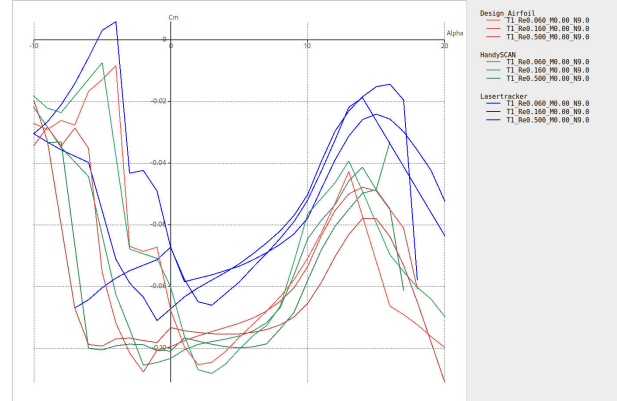


FIG. 24. Plot of the polars of the pitching moment coefficient to the angle of attack at the wing

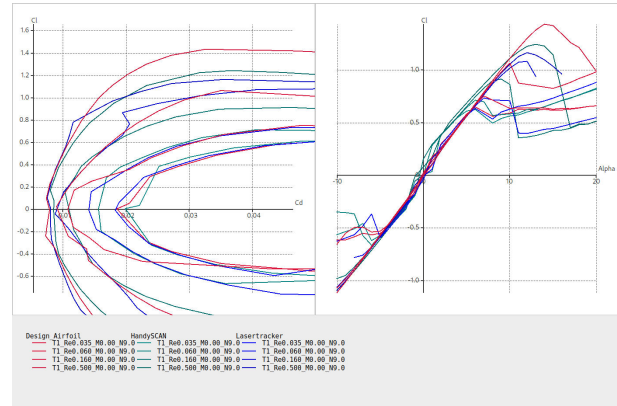


FIG. 25. Comparison of the polars of the v-tail to the design profile at four different Reynolds numbers

especially at a Reynolds number of $5 \cdot 10^5$. However, this high number is unlikely to be reached in flight, and is therefore less relevant. When comparing the α_{max} -value, the section of the *HandySCAN 700* data always has similar values as the design airfoil, and for the section of the Lasertracker this value is shifted to a higher or lower angle of attack. However, the $c_{l,\alpha}$ -coefficient is approximated better by the section of the Lasertracker. Overall, both airfoils exhibit a comparable aerodynamic behavior to the design airfoil if the Reynolds number is not too high.

The pitching moment coefficient of both compared airfoils stays within the same area as the one of the design airfoil. Especially for negative α -values, the derivative is approximated well. The Lasertracker generates better results than the *HandySCAN 700*, possibly because of the similar thickness of the generated airfoil compared to the design airfoil. This plot is presented in Fig. 26.

4.3.3. Aerodynamic Behavior of the Vertical Tail

Only a section of the *HandySCAN 700* was compared to the design airfoil for the vertical tail. The solution did not converge for high values of the angle of attack. However, similar tendon-

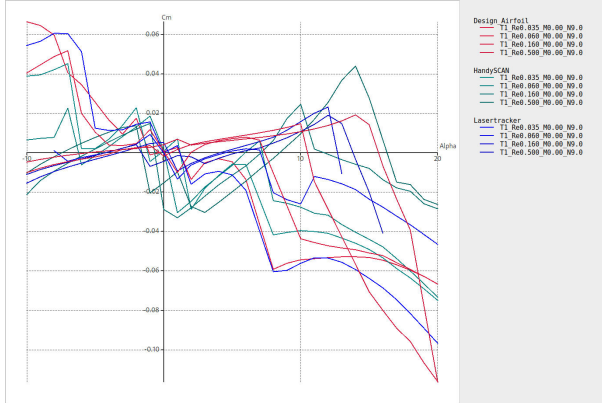


FIG. 26. Plot of the polars of the pitching moment coefficient to the angle of attack at the v-tail

cies can be observed on both airfoils (see Fig. 27), and high angles of attack will not be reached during flight.

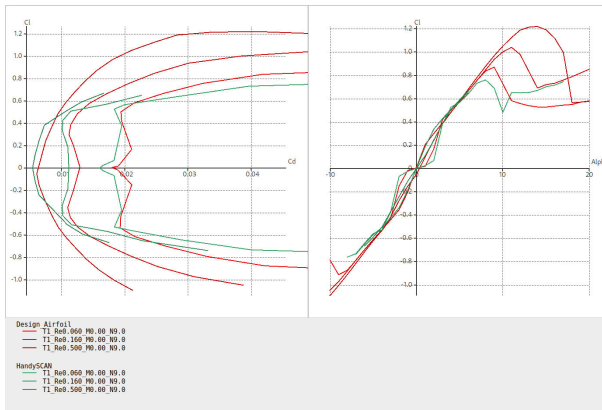


FIG. 27. Comparison of the polars of the vertical tail to the design profile at three different Reynolds numbers

4.4. Influence of the Fitting Process on the aerodynamic Behavior

To check how the fitting influences the aerodynamic behavior, polars for a non-fitted airfoil were computed and compared to polars of a fitted airfoil and the design airfoil. The extracted airfoil had no adequate resolution at the leading edge, so XFLR5 generated a pointy leading edge. A fourth section was generated using a global refinement in the Direct Design Toolbox of XFLR5. The points of the non-fitted section were redistributed to form a round leading edge. The results of the computation are shown in Fig. 28.

The non-fitted and non-refined section of the scan only resembles the design airfoil between a c_l -value of 0.4 to 1.2. Above and below, there are significant differences. However, the refined section approximates the design airfoil well, even better than the fitted airfoil. This can be explained by the low resolution of the leading edge. The leftmost point is used to separate the airfoil into lower and upper halves and also de-

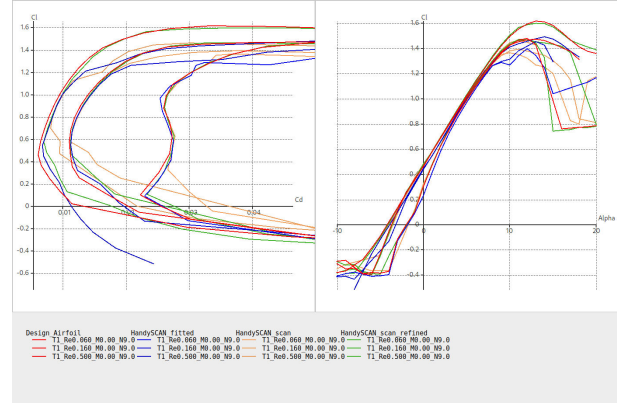


FIG. 28. Comparison of the polars of three different Reynolds numbers with the design profile

fines the coordinate origin. If this point is not near the actual leading edge, the airfoil is incorrectly separated and translated (see Fig. 29).

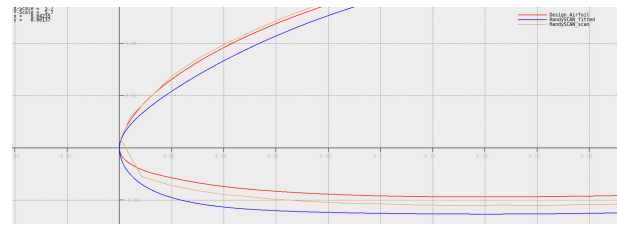


FIG. 29. Zoom to the leading edge of the compared airfoils

5. ASSESSMENT OF THE FUSELAGE SECTION

5.1. Abilities of the Fitting Process

There is also a routine to fit the fuselage. Three options are available, a circular, ellipsoidal and superellipsoidal fitting. The superellipse is described by Eq. 3. Here, a and b define the half axes of the superellipse and ϵ is the shape factor. For $\epsilon = 2$, the equation becomes the standard ellipse equation. For $\lim_{\epsilon \rightarrow \infty}$ the equation describes a rectangle, for $\epsilon = 1$ a diamond, and for $\epsilon < 1$ a cross. The three fitting methods are presented in Fig. 30 to 32.

$$(3) \quad S(x, y) = \left| \frac{x}{a} \right|^{\frac{2}{\epsilon}} + \left| \frac{y}{b} \right|^{\frac{2}{\epsilon}} = 1$$

For the circular fitting, the mean length of the width and height of the fuselage is chosen as diameter for the fitting. For an ellipse, the width is interpreted as a and the height as b (see Eq. 3). The superellipse fitting is an iterative process where ϵ -values between 0 and 50 are tested to minimize the absolute difference. This fails if the section cuts more than the actual fuselage, e.g. parts of the wing or any gadget mounted on the aircraft (see Fig. 33).

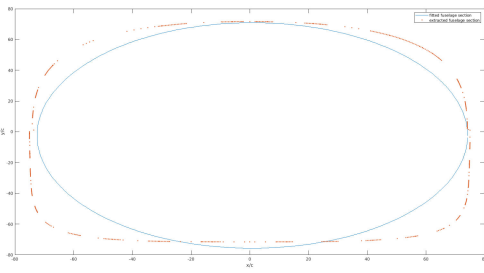


FIG. 30. Circular fitting of the fuselage

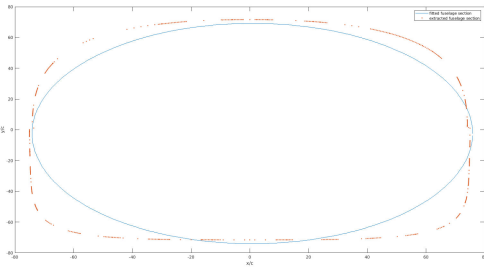


FIG. 31. Ellipsoidal fitting of the Fuselage

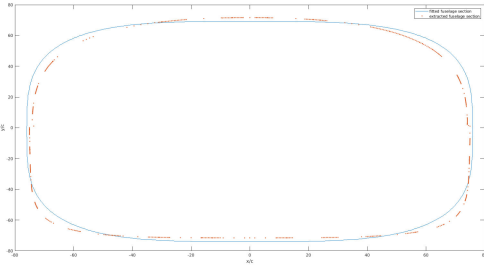


FIG. 32. Superellipsoidal fitting of the fuselage

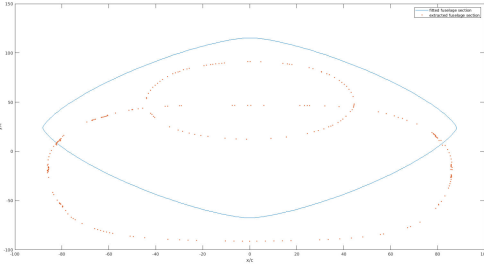


FIG. 33. Failing of the fuselage fitting

5.2. Assessment of a Fuselage Section

The only 3D-scan containing a complete fuselage is the one generated using the *HandySCAN 700*. For the other scanners, the fuselage cover was removed to get a horizontal

edge. A section of this scan was chosen and fitted with the superellipse process. The plots of the fuselage and its absolute difference is shown in Fig. 34.

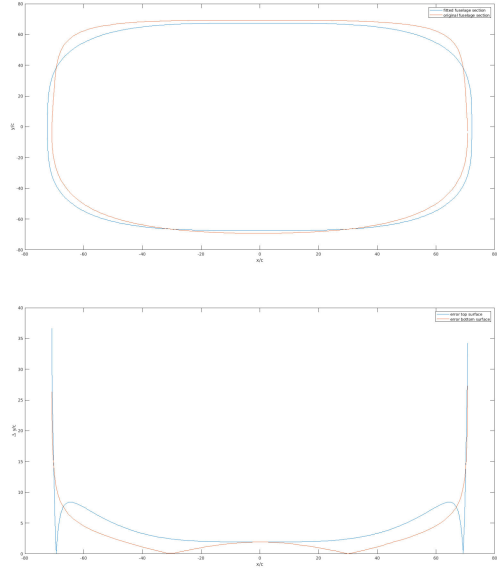


FIG. 34. Top: Comparison of the fuselage section at 180 mm, generated by the *HandySCAN 700*, to the design fuselage. Bottom: The absolute difference in y-direction between both fuselages.

It can be seen that the approximation by the superellipse does not fit the designed fuselage completely. The reason for this deviation is the cover of the fuselage. The cover has no rigid structure, so its original shape can be easily distorted. The mean distance is 6.36 mm and the absolute difference is 36.698 mm. However, these values are not directly comparable because only the difference in y-direction is accounted for. For more meaningful values, the quadratic distance between the two curves has to be computed. This would also reduce the maximum distance significantly.

6. RECONSTRUCTION OF THE AIRCRAFT

All point clouds were sectioned and geometric characteristics were extracted. The characteristics contain values like the dihedral, chord length and twist. As an example, a CAD model and a model in XFLR5 of the aircraft was reconstructed using all this data. The used point cloud is the one of the *HandySCAN 700*, in order to be able to reconstruct the fuselage as well. These reconstructions and the extracted characteristics are compared in the following section.

6.1. Comparison of the geometric Characteristics

The geometric characteristics of the wing of all scans are compared to the design values. The compared values are the chord length, the dihedral, the twist and the offset of the leading edge. Even if sections could not be fitted, some char-

acteristics of the sections can be compared since these are independent of the scanning resolution.

6.1.1. Chord Length

The following table presents the results of the chord length in millimeter (see Tab. 4). The sections at the wing tip show a significant greater value than the one of the design model. However, the wing tip was later revised to ensure enough space for the motor. The remaining values match the design values within a few millimeters. Interestingly, the computed chord lengths of the first Lasertracker sections are significantly shorter than the ones of the *HandySCAN 700* sections. The scan of the *RTC360* also provides similar lengths as the Lasertracker. The reason for this discrepancy is unclear.

Sectioning Distance [mm]	Design [mm]	Handy-SCAN 700 [mm]	Laser-tracker [mm]	RTC360 [mm]
110	299.604	300.062	294.16	292.419
350	293.354	294.007	288.84	287.703
675	273.592	275.97	272.67	267.145
1010	235.962	239.761	238.908	233.632
1150	213.786	216.822	216.888	-
1350	168.748	173.755	170.265	-
1425	147.972	154.964	152.169	-
1450	138.862	154.991	149.571	-

TAB. 4. Comparison of the chord length of the extracted sections to the design characteristic

6.1.2. Dihedral

The dihedral of the aircraft is expected to be smaller than the one of the design aircraft, since gravity deflects the wings downwards. The results in degrees are presented in Tab. 5. As can be seen, the dihedral is about 2 degrees smaller at the wing root. Towards the wing tip, the dihedral increases but never reaches the value of the design characteristic. The dihedrals of the values of the three scans differ to some degree. This can be explained by the surface resolution of the different scans. Normal vectors on the surface are computed and averaged to compute the dihedral of the airfoil section.

6.1.3. Twist

The extracted twist value is a combination of the tilt angle and the twist of the design airfoil, since it is impossible to extract them both. No leading or trailing edge could be reliably found for the *RTC360*, so its twist could not be extracted. As several surfaces were tracked in the 3D-scan of the Lasertracker (see Sec. 4.2.1), that twist value is not comparable as well. The comparison of the scan of the *HandySCAN 700* to the design model is presented in Tab. 6.

Sectioning Distance [mm]	Design [°]	Handy-SCAN 700 [°]	Laser-tracker [°]	RTC360 [°]
110	2	0.012	0.352	0.345
350	2	0.022	0.456	0.797
675	2	0.445	0.844	0.397
1010	2	0.499	1.005	1.452
1150	2	0.619	0.784	-
1350	2	1.141	1.2	-
1425	2	1.081	2.657	-
1450	2	1.788	1.878	-

TAB. 5. Comparison of the dihedral of the extracted sections to the design characteristic

Sectioning Distance [mm]	Design [°]	Handy-SCAN 700 [°]
110	3.74	2.715
350	3.59	2.818
675	3.37	2.29
1010	3.15	2.377
1150	3.05	-3.088
1350	2.92	2.229
1425	2.87	2.582
1450	2.85	2.841

TAB. 6. Comparison of the twist of the extracted sections to the design characteristic

The twist is reduced to the wing tip, just as in the design model. However, the last two sections again contain a higher twist angle. This can be again explained by the revised airfoils containing the motor of the wing tip. The twist can slightly differ from the design airfoil, since it can not be guaranteed that the middle point of the trailing edge is chosen for the rotation.

6.1.4. Offset

For the offset, all scanners can be compared. However, their coordinates have to be compared carefully as well. The alignment of the main axes does not determine the direction of the aircraft (see [2]). Thus, it is unknown whether the leading edge is the leftmost or rightmost point of the airfoil. A routine was designed to find the leading edge, if the points on the airfoil are distributed evenly across the section. If there are many points on the trailing edge, this routine fails and returns the trailing edge instead of the leading edge. Therefore, values greater than the chord length can be found in this section. However, these values can be corrected by reducing the chord length (see Tab. 7).

Additionally, the offset of the sections can only be calculated beginning from the first section. Therefore, all values reference the first leading edge (or trailing edge) of the first section. The values of the Lasertracker and the *RTC360* are not completely reliable, since both leading edges could not be defined

completely. As for the *HandySCAN 700*, the values of the offset are significantly higher than the design characteristic. Whether this deviation is caused by the high manufacturing tolerances can not be determined.

Sectioning Distance [mm]	Design [mm]	Handy-SCAN 700 [mm]	Laser-tracker [mm]	RTC360 [mm]
110	0.206	0	0	0
350	1.974	4.017	288.833 (0.0)	288.718 (1.018)
675	7.564	11.462	1.385	272.592 (5.447)
1010	18.21	24.35	247.025 (8.117)	247.355 (13.723)
1150	24.484	248.364 (31.542)	229.974 (13.086)	-
1350	37.225	45.858	194.239 (23.974)	-
1425	43.103	50.266	179.214 (27.045)	-
1450	45.68	48.799	25.722	-

TAB. 7. Comparison of the offset of the extracted sections to the design characteristic

6.2. Reconstruction in CATIA V5

All sections of the *HandySCAN 700* were imported to CATIA V5 for a reconstruction of the aircraft. The sections were rotated according to their dihedral and twist, and a surface was interpolated between the sections. The sectioning can only be done within some distance between the root and tip of the lifting surfaces. This results in separated parts which represent the main bodies of the aircraft. A comparison to the design CAD model as well as the resulting histogram is shown in Fig. 35. It was filtered to only show a difference of ± 5 mm, which corresponds to 90.5% of the actual model.

The difference between the reconstructed model and the reference CAD model is larger than the difference between the scanned data and the reference model. The filtered areas are the position of the rear rotor gondola and the wing tip. The difference at the fuselage results from the reconstruction process. All fuselage sections, as well as the section at the gondola, were fitted to superellipses. Afterwards, a surface was constructed using all fitted sections. Using this process, small discontinuous areas are ignored and smoothed. The wing tip contains only a small amount of scanned points due to its dark color. This part of the wing could not be exported as accurately as the rest of the point cloud.

The deviations mostly stay between -1.5 mm and 3.5 mm and include all manufacturing and scanning tolerances, and potential inaccuracies of the toolchain. The slightly worse results than the one of the 3D-scan are explained by fitting problems as described in Sec. 4.1.

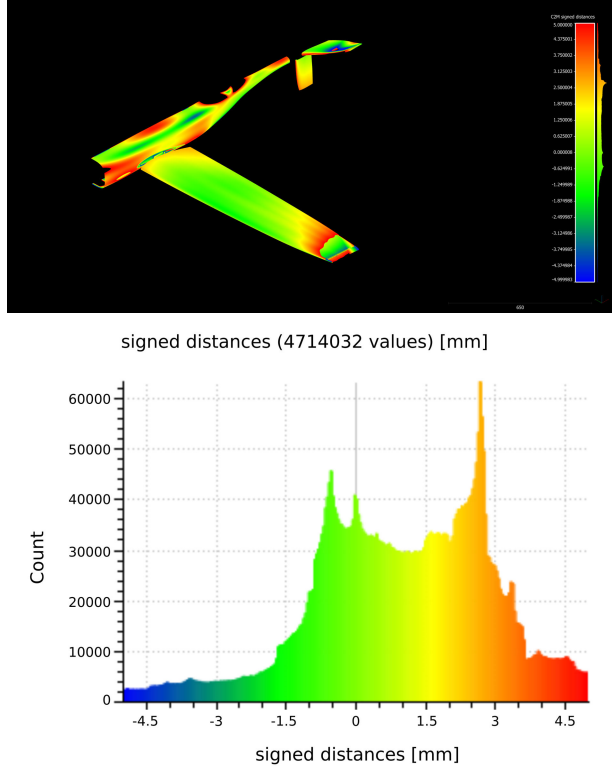


FIG. 35. Comparison of the reconstructed CAD model to the design CAD model

6.3. Reconstruction in XFLR5

The same sections as in the Catia V5 model were chosen to generate the XFLR5 model. The model is presented in Fig. 36.

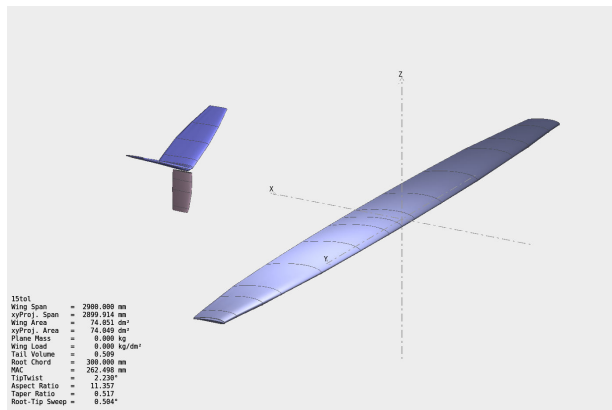


FIG. 36. Reconstructed model in XFLR5

Since the resolution in direction of the wing tip decreases significantly, the wing can not be sectioned at the very edges. This results in the generated wing and tail area being smaller than the one of the design aircraft. Additionally, the number of sections has an influence on this value. The reconstructed wing area is 74.05 dm², while the design area is 75.01 dm².

The wing span is reduced from 3000 mm to 2900 mm, and the volume of the tail decreases about 7%.

For the comparison, exported sections of the CATIA V5 model were integrated into the design model of XFLR5. Next, polars for a flight with constant airspeed of 10 m/s, 15 m/s and 20 m/s were computed for both models. The results are presented in Fig. 37.

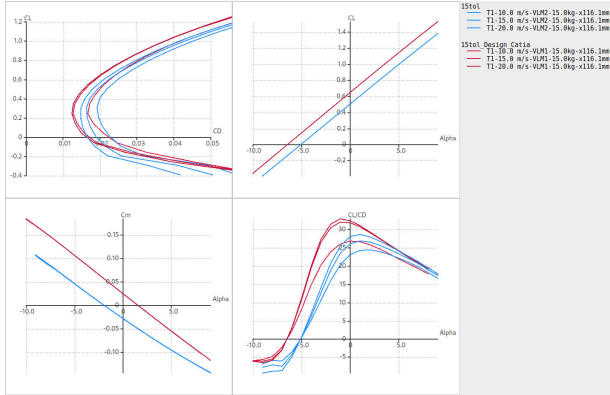


FIG. 37. Comparison of the polars for the CATIA V5 and the XFLR5 model

The polars differ significantly. However, the value of $c_{D,0}$ could be exactly represented for the flight with 10 m/s and 20 m/s. Above, the drag coefficient is significantly higher than the one of the design airfoil. This can be explained by a faulty fitting. Since points of the trailing edge could not be deleted several times, the airfoils are thickened, which creates a higher drag. The quality of the scan and the fitting process also influences the overall lift coefficient. The $c_{m\alpha}$ -value of both aircraft are identical to an angle of attack of 5°. Afterwards, the curve of the reconstructed aircraft flattens.

Most of the deviations are explained by the incomplete scanning of the foil, or a faulty fitting afterwards. This can be seen in Fig. 38, where the reconstructed airfoil was refined such that all sections were replaced by the root section of every lifting surface.

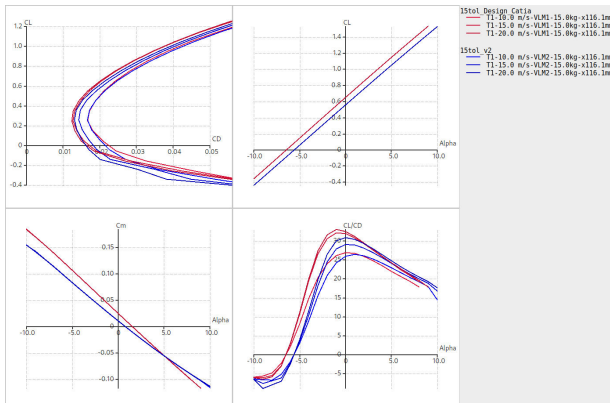


FIG. 38. Comparison of the refined reconstructed airfoil to the design aircraft

This relatively small refinement results in a significantly better representation of the design aircraft. In general, a higher lift coefficient was achieved. In addition, the drag coefficient was reduced, such that the polars mostly match each other and the $c_{m,0}$ -value was also increased. Only the $c_{m\alpha}$ derivative was slightly changed.

7. CONCLUSION

In conclusion, the quality of the extraction tools is highly dependant on the quality of the available 3D-scans. An overall comparison of a complete aircraft to the CAD design model is of only limited usefulness. If manufacturing tolerances are high, like the ones of the 15tol, deviating characteristics and the static distortion of the aircraft degrade the results, as well as the distances between the point clouds. Therefore, it can sometimes be more helpful to just compare a part of the aircraft, e.g. the wing. For the HandySCAN 700, there is a significant improvement in the resolution if the MAXshot 3D system is used for the assistance model generation.

For a successful fitting, the sections should be of the best resolution possible. Points on the trailing edge were the most common error to show a worse result than the original scan. If that is the case and the section should be compared anyway, these points have to be deleted manually before trying to fit the section. However, geometric deviations do not play a major role in the aerodynamic behavior. More important are the position and thickness of the leading edge, which has to be scanned very carefully. Since a good resolution of the leading edge can not be guaranteed, the fitting is a good option for refining the results in this area and improving the aerodynamic behavior. Nonetheless, the section has to contain at least one point near the actual leading edge for the fitting to work well. The fitting of the fuselage is more robust than the fitting of the wing and tail. Deviations of a flexible cover can be compensated. However, the exact form of the fuselage might be impossible to model if the deviations from the design geometry are too great, and ellipsoidal and circular fitting will most likely result in a smaller fuselage area than the original one.

The generated characteristics have similar values compared to the reference design, but it can not be determined completely where these deviations ultimately result from. However, when used for reconstruction of the aircraft, most of the values are usable and the reconstructed CAD model had a similar shape as the design CAD model. The tolerances are a bit higher than the original 3D-scan, but within the range of the manufacturing tolerances. However, both models are not completely comparable because transitions between lifting surfaces and the fuselage can not be modeled. The missing wing tips complicate a comparison as well.

Even if the tips could not be sectioned, the reconstructed model has a similar aerodynamic behavior. However, a requirement for this is that only the best fitted airfoils (especially with a pointy trailing edge) are chosen for the representation. To be able to choose the best sections, generating a high number of sections is recommended. This also improves the wing area of the XFLR5 model.

Overall, the toolchain is capable of extracting plausible values and sections from the 3D-scan. Even though all sections and

values should be checked beforehand, they can be used to generate a similar model in a CAD software, as well as in low-fidelity tools like XFLR5.

8. OUTLOOK

In [2], the UAV *DG-800* was extracted to test the algorithm, using an aircraft with unknown geometry. In the future, this will become the main area of application: Reconstructing aircraft with unknown shapes in e. g. XFLR5 and comparing the computed coefficients to the ones gained by flight testing. To validate the improvements of the toolchain, the *DG-800* was sectioned again, using the refined implementation. The aerodynamic behavior of one section was compared and is presented in Fig. 39.

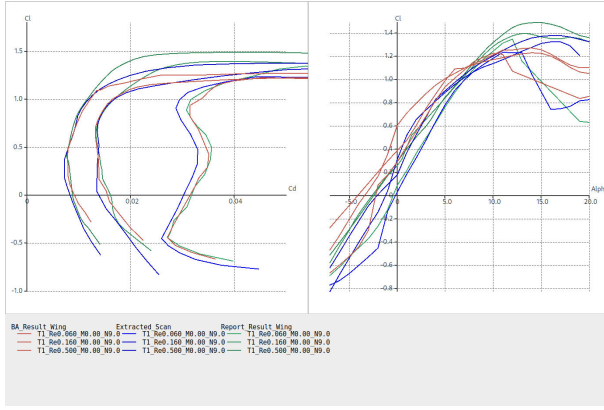


FIG. 39. Comparison of the aerodynamic behavior of a section of the *DG-800* extracted with the old as well as the refined toolchain, and a non-fitted section for three different Reynolds numbers

The airfoil extracted using the refined toolchain generates the highest lift coefficients. All airfoils converged to high angles of attack, and the c_{l_α} -value is comparable as well. Since the non-fitted α_{max} -value is roughly the same as the one of the refined toolchain, the smoothing was successful and the airfoil should provide a good approximation of the design airfoil. Ultimately, the refinement of the toolchain is considered successful.

9. ACKNOWLEDGEMENT

We thank the Institute of Geodesy for providing the 3D-scans of the *RTC360* and the Lasertracker. Without these scans, this report could not have covered some of the open questions regarding the 3D-scanning point cloud extractor.

10. REFERENCES

- [1] Kaan Mustafa Çetin. *Development and Implementation of a 3D-Scanning-Toolchain for the Characterization of UAVs*. Bachelor's thesis, Technical University Munich, 2020.
- [2] Lina van Brügge. *Development and Implementation of a 3D-Scanning-Toolchain for the Geometric Characterization of UAVs*. Bachelor's thesis, Technical University Munich, 2020.
- [3] Lina van Brügge, Kaan Çetin, Sebastian Köberle, Moritz Thiele, Fabian Sturm, and Mirko Hornung. Application of 3D-Scanning for Structural and Geometric Assessment of Aerospace Structures. In *Deutscher Luft- und Raumfahrtkongress 2021*, 2021.
- [4] CloudCompare, 3.5.2022. URL <https://www.cloudcompare.org/main.html>.
- [5] CATIA V5, 3.4.2022. URL <https://www.3ds.com/de/produkte-und-services/catia/>.
- [6] XFLR5, 3.4.2022. URL <http://www.xflr5.tech/xflr5.htm>.